Supplementary Information

Tuning the spin polarization in monolayer MoS_2 through (Y, Yb) co-doping

Yong Niu,[a,b] Pan Wang,*[a,b] and Mingzhe Zhang[c]

[a]Research Center for Semiconductor Materials and Devices, Shaanxi University of Science and Technology, Xi'an 710021, China

[b]Department of Physics, Shaanxi University of Science and Technology, Xi'an 710021, China

[c]State Key Laboratory of Superhard Materials, Jilin University, Changchun 130012, China

* Corresponding Author. E-mail: wangpan.chen@163.com

1. Models for monolayer MoS_2 with single Y dopant, Yb dopant, and native defects

To explain the mechanism of the impact of single Y dopant, single Yb dopant, and native defects on spin polarization in monolayer MoS_2, first-principles calculations were performed. The single Y dopant (replacing one Mo atom by a Y atom) (Figure S1a), single Yb dopant (replacing one Mo atom by a Yb atom) (Figure S1b), and native defects were investigated. In S-rich condition, the main native defects are three cases (Figure S1c-e): (1) one Mo vacancy defect (V_{Mo}); (2) one S interstitial defect (S_i); (3) one S antisite defect (S_{Mo}), severally. In Mo-rich condition, the main native defects are

two cases (Figure S1f-g): (1) one S vacancy defect (V_S); (2) one Mo antisite defect (Mo_S), respectively.

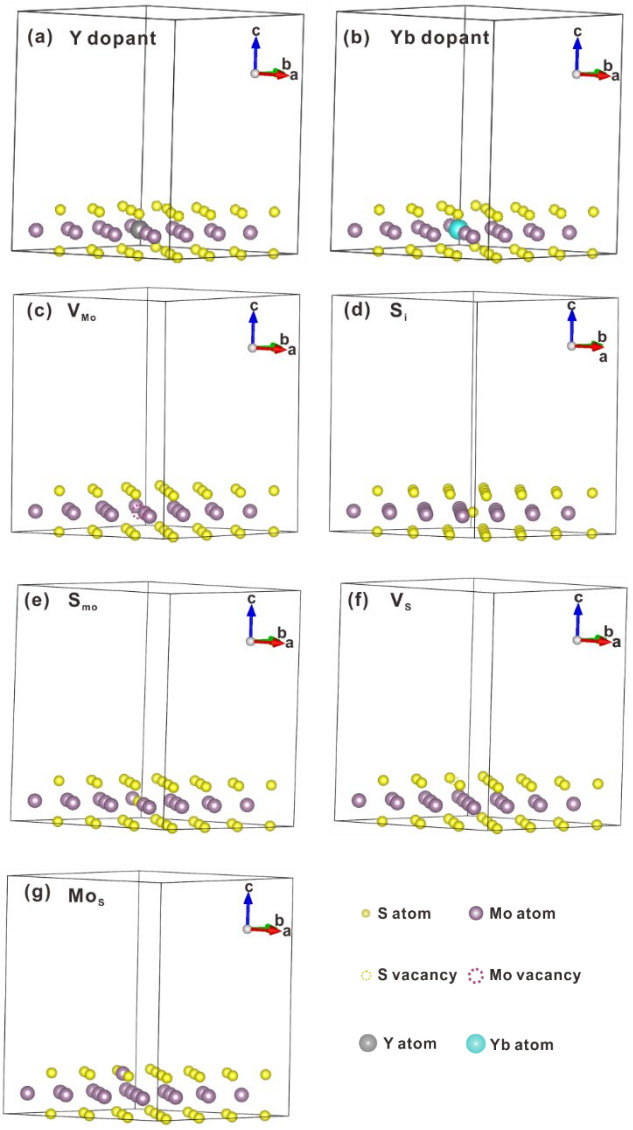

Figure S1. The model configuration of the 4×4×1 2D monolayer MoS_2 supercells with various dopants and defects. (a) Y dopant (Y_{Mo}); (b) Yb dopant (Y_{Mo}); (c) Mo vacancy (V_{Mo}); (d) S interstitial defect (S_i); (e) S antisite defect (S_{Mo}); (f) S vacancy (V_S); (g) Mo antisite defect (Mo_S).

2. U value of Yb, Y and Mo atom

According to the previous theoretical calculation study on 4f orbitals of lanthanide atoms with GGA+U calculation, when U value was increased from 0 to 7 eV, it was found that geometrical structure had no significant change, but 4f states started to become localized for U > 4 eV.[1] Moreover, the U value of lanthanide atoms was usually set to 6 eV to perform the GGA+U calculation.[2, 3] As reported by this work (Zs. Rák & D.W. Brenner (2015) Philosophical Magazine, 95:20, 2167-2174)[4], the multiple values of 5.44, 6.75 and 8.16 eV were used for Yb 4f. Therefore, U values of 5 eV, 6 eV, and 7 eV were applied to the Yb 4f orbital to choose the best U value in favor of the lowest total energy and the correct electronic structure for Yb doped monolayer MoS_2. As displayed in Figure S2, the calculated DOS results of Yb doped monolayer MoS_2 with different U values of Yb 4f orbital are basically consistent, and U=5 eV is in favor of the lowest total energy and highest magnetic moment for Yb doped monolayer MoS_2 as displayed in Table S1. Therefore, U=5 eV is applied to Yb 4f orbital.

The calculation result of density of states (DOS) of Y doped monolayer MoS_2 without "+U" correction of Y 4d electron displayed in Figure S3 is basically consistent with the other U values of Y4d. Moreover, the calculated total magnetic moments of Y doped monolayer MoS_2 supercell for U = 0 eV, 2 eV, 3 eV, 4 eV, and 5 eV of Y 4d orbital are all equal to zero, and U=0 eV is in favor of the lowest total energy for Y doped monolayer MoS_2 as displayed in Table S2. Therefore, there is no U correction for Y 4d electrons.

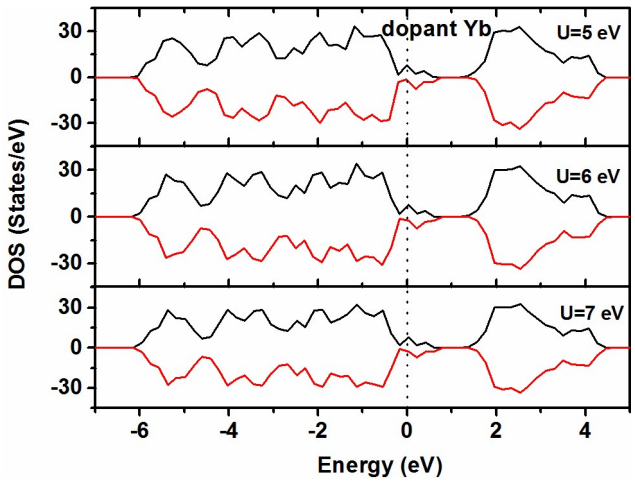

Figure S2. The calculated DOS of Yb doped monolayer MoS_2 supercell for U = 5 eV, 6 eV, and 7 eV of Yb 4f, respectively. The Fermi level (E_F=0 eV) is indicated by the black dotted vertical line.

Table S1. The energy and total magnetic moment of Yb doped monolayer MoS_2 for U = 5 eV, 6 eV, and 7 eV of Yb 4f, respectively.

U (eV)	E (eV)	M (μ_B)
5	-335.72492	1.18
6	-335.61836	1.15
7	-335.53355	1.10

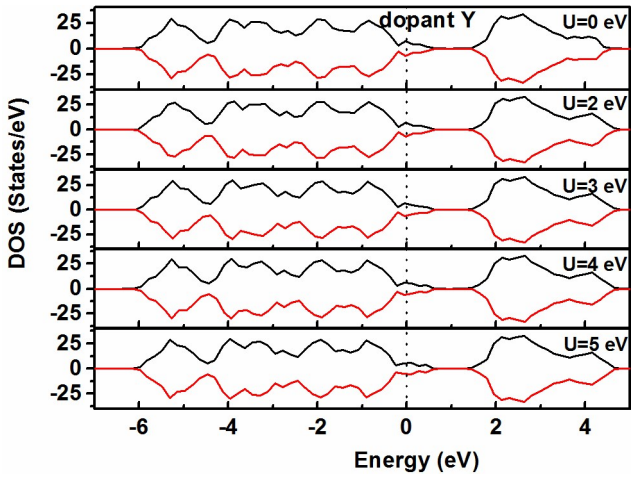

Figure S3. The calculated DOS of Y doped monolayer MoS_2 supercell for U = 0 eV, 2 eV, 3 eV, 4 eV, and 5 eV of Y 4d, respectively. The Fermi level (E_F=0 eV) is indicated by the black dotted vertical line.

Table S2. The energy and total magnetic moment of Y doped monolayer MoS_2 for U = 0 eV, 2 eV, 3 eV, 4 eV, and 5 eV of Y 4d, respectively.

U (eV)	E (eV)	M (μ_B)
0	-342.62183	0.00
2	-341.69425	0.00
3	-341.25112	0.00
4	-340.82264	0.00
5	-340.40868	0.00

3. Spin-polarized DOS of the monolayer MoS_2 with native defects

To get a deeper understanding of the role of native defects at S-rich condition in modulating spin polarization of monolayer MoS_2, the spin-polarized DOS of the three monolayer MoS_2 systems with one Mo vacancy, S interstitial defect, and S_{Mo} antisite defect were computed and compared, as shown in Figure S4a-c, respectively. The models of monolayer MoS_2 with one Mo vacancy, S interstitial defect, and S_{Mo} antisite defect are presented in Figure S1 (c), (d) and (e), respectively. In case of one Mo vacancy (Figure S4a), the spin-up and spin-down DOS are symmetric leading to zero spin polarization and magnetic moment. In contrast to the ideal monolayer MoS_2, Mo vacancy brings up the shallow acceptor levels similar to Y dopant, which primarily develops from the surrounding holes trapped by the Mo vacancy with negative

electricity. For S interstitial defect (Figure S4b), impurity donor levels (stressed by the red circles) are only brought in the spin-up channel close to the bottom of the conduction band mainly composed of the S 2p orbitals, which gives rise to a total magnetic moment of 1.19 μB. As depicted in Figure S4c, owing to the symmetric total spin-polarized DOS for the case of the S_{Mo} antisite defect, no spin polarization and magnetic moment come out. Contrasting with the perfect monolayer MoS_2, S_{Mo} antisite defect brings up two impurity states at the top of the valence band and brings up one impurity state at the bottom of the conduction band, which are all mainly contributed by the coupling between S 2p and Mo 4d orbitals.

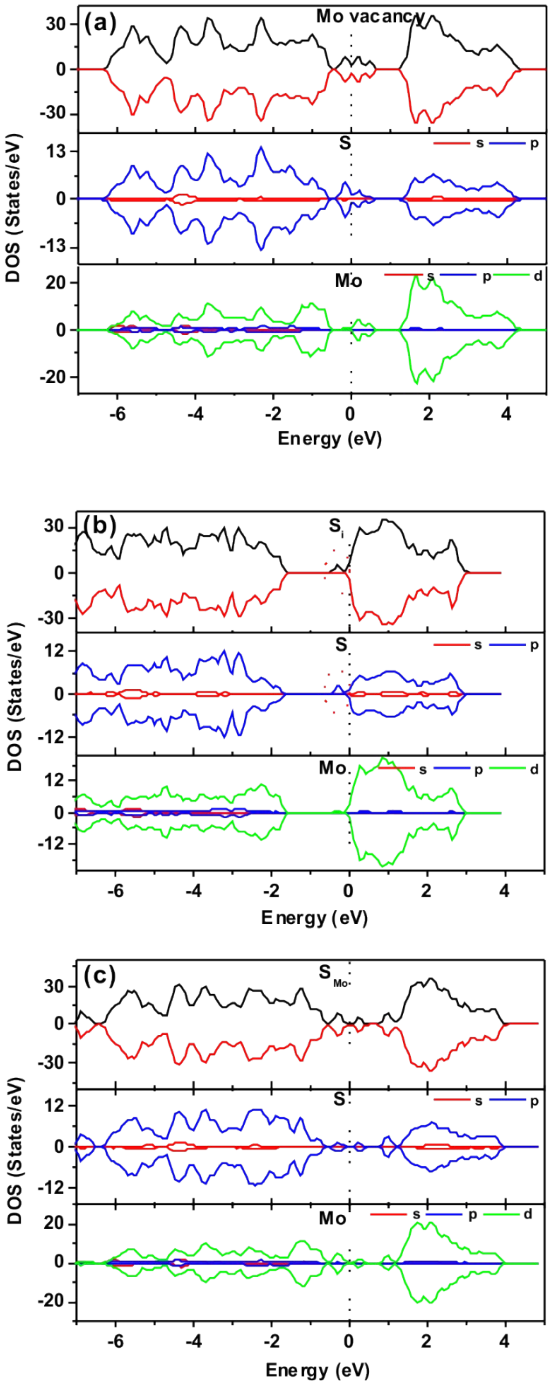

Figure S4. Spin-polarized total and partial DOS of four native defective monolayer MoS_2 cases in S-rich condition: (a) a Mo vacancy, (b) a S interstitial defect, and (c) a S_{Mo} antisite defect, respectively. The black dotted vertical line and red circles mark the position of the Fermi level (E_F=0 eV) and the split positions of the spin-polarized DOS, respectively.

The influence of the native defects in Mo-rich condition on the spin polarization of monolayer MoS_2 was also investigated. The models of monolayer MoS_2 with one S vacancy and Mo_S antisite defect are demonstrated in Figure S1 (f) and (g), respectively. The spin-polarized DOS of the two defective monolayer MoS_2 systems is depicted in Figure S5a-b, respectively. As displayed in Figure S5a, S vacancy defect does not generate the spin polarization and magnetic moment, and only produces an impurity donor band which mainly originates from Mo 4d orbitals below the bottom of the conduction band. For Mo_S antisite defect (Figure S5b), half-occupied defect states occur in spin-up channel close to the bottom of the conduction band crossing the Fermi level which mainly is the result of the Mo 4d orbitals, whereas the spin-down channel basically maintains the broad band gap similar to the ideal monolayer MoS_2 (Figure 1b), which is consistent with previous theoretical report on Mo_S antisite defect in monolayer MoS_2[5], eventually resulting in a typical half-metallic character with the magnetic moment of 2.00 μB. Therefore, spin polarizations in monolayer MoS_2 can also be induced by S interstitial and Mo_S antisite defects, and Mo_S antisite defect contributes the highest spin polarization in contrast to other defects.

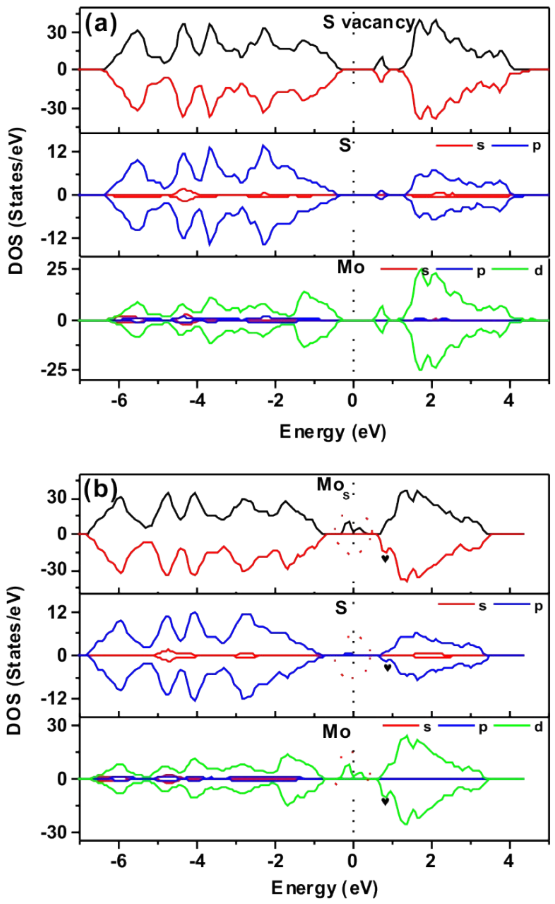

Figure S5. Spin-polarized total and partial DOS for two native defective monolayer MoS_2 cases in Mo-rich condition (a) with a S vacancy, (b) with a Mo_S antisite defect. The black dotted vertical line and red circles mark the position of the Fermi level (E_F=0 eV) and the split positions of the spin-polarized DOS, respectively.

4. The energy difference (ΔE) between AFM and FM states of (2Yb, Y) co-doped monolayer MoS_2

As shown in Table 1 of energy difference (ΔE) between AFM and FM states of 2Yb doped MoS_2 monolayer in different configurations, the (0, 1), (0, 3) and (0, 4) configurations constructed by fixing one of the couple of Yb dopants at position Yb0 and another substituted Yb atom at Mo atom site marked with Yb1, Yb3, Yb4, respectively, are all in favor of the ferromagnetic states. The remaining FM (0, 3) and

(0, 4) configurations with one Y dopant at different positions were also calculated and discussed as follows.

As shown in Figure S6a, two Yb atoms are fixed at Yb0 and Yb3 positions, and single Y atom substitutes for one Mo atom at positions labelled by Y_1, Y_2, Y_3, Y_4, Y_5, Y_6, Y_7, Y_8, Y_9, Y_{10}, Y_{11} to construct eleven configurations D1, D2, D3, D4, D5, D6, D7, D8, D9, D10, D11, respectively. As shown in Figure S6b, two Yb atoms are fixed at Yb0 and Yb4 positions, and single Y atom substitutes for one Mo atom at positions labelled by Y_1, Y_2, Y_3, Y_4, Y_5, Y_6, Y_7, Y_8 to construct eleven configurations E1, E2, E3, E4, E5, E6, E7, E8, respectively. The calculated results of total energy difference ΔE between AFM and FM states for the above configurations are listed in Table S3 and S4. From Table S3 and S4, the energy differences ΔE of D4 and E3 configurations are the largest, indicating that FM couplings are more stable in energy than the AFM couplings in D4 and E3 cases.

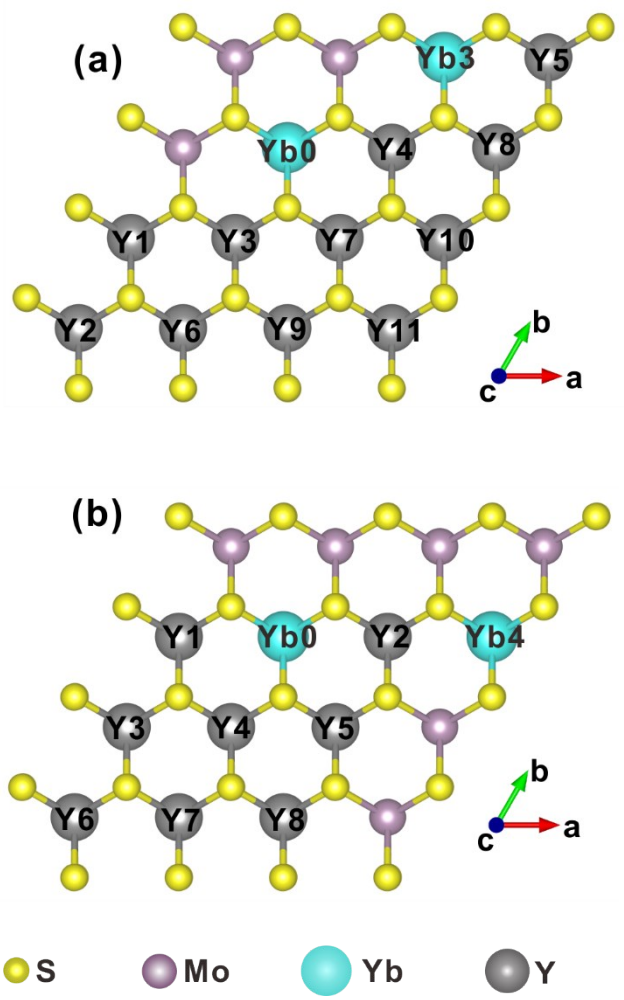

Figure S6. Top view of the 48-atom 4×4×1 supercell model of monolayer MoS_2 (a) with two Yb dopants at Yb0 and Yb3 position, and one Y dopant denoted by Y1-Y11, respectively; (b) with two Yb dopants at Yb0 and Yb4 position and one Y dopant denoted by Y1-Y8, respectively.

Table S3. The energy and total magnetic moment of FM and AFM states, energy difference (ΔE) between AFM and FM states, and stable magnetic ground state (MS) for eleven configurations of monolayer MoS_2 with two Yb dopants at Yb0 and Yb3 position, and one Y dopant denoted by Y1-Y11, respectively.

Model	FM		AFM		ΔE (meV)	MS
	Energy (eV)	Moment (μ_B)	Energy (eV)	Moment (μ_B)		
D1	-314.63955	0.96	-316.71484	0.36	-2075.29	AFM
D2	-309.37428	6.20	-317.09627	-0.87	-7721.99	AFM
D3	-317.12059	0.94	-316.79195	-0.69	328.64	FM
D4	-329.06024	-0.14	-317.93821	-0.01	11122.03	FM
D5	-319.08325	1.91	-317.81700	0.04	1266.25	FM
D6	-313.25424	-0.86	-317.69706	0.48	-4442.82	AFM
D7	-308.62407	-0.12	-316.98077	0.16	-835.67	AFM
D8	-316.79473	0.58	-317.71979	0.62	-925.06	AFM
D9	-328.23509	0.96	-317.75465	0.26	10480.44	FM
D10	-312.66259	1.33	-317.13984	0.00	-4477.25	AFM
D11	-317.84165	0.20	-316.67207	0.03	1169.58	FM

Table S4. The energy and total magnetic moment of FM and AFM states, energy difference (ΔE) between AFM and FM states, and stable magnetic ground state (MS) for five configurations of monolayer MoS_2 with two Yb dopants at Yb0 and Yb4 position, and one Y dopant denoted by Y1-Y8, respectively.

Model	FM		AFM		ΔE (meV)	MS
	Energy (eV)	Moment (μ_B)	Energy (eV)	Moment (μ_B)		

E1	-317.26052	-1.05	-317.71955	0.07	-459.03	AFM
E2	-324.26064	-1.09	-317.72176	-0.10	6538.88	FM
E3	-329.94473	1.83	-316.84674	-0.49	13097.99	FM
E4	-315.08001	3.88	-317.60194	-0.40	-2521.93	AFM
E5	-315.97818	3.63	-317.46224	0.47	-1484.06	AFM
E6	-314.35335	-0.52	-316.50131	0.77	-2147.96	AFM
E7	-317.28742	0.23	-315.40023	0.03	1887.19	FM
E8	-316.04763	2.61	-316.50810	-0.07	-460.47	AFM

5. The effect of Yb/Y dopant on Mo_S antisite defect formation energy

Owing to Mo_S antisite defect in favor of the highest spin polarization in contrast to the other defects, the effect of Y/Yb dopant on the Mo_S antisite defect formation energy was studied. Defect formation energies of the Mo_S antisite defect for the monolayer $Mo_{17}S_{31}$ with one Mo_S antisite, $Mo_{16}YS_{31}$ with one Mo_S antisite and one Y dopant, $Mo_{16}YbS_{31}$ with one Mo_S antisite and one Yb dopant are calculated.

For pristine monolayer MoS_2, the chemical potentials μ_{Mo} and μ_S must meet the condition as follows [6]:

$$\mu_{MoS_2} = \mu_{Mo} + 2\mu_S \quad (1)$$

where μ_{MoS_2} is the total energy of the pristine monolayer MoS_2. In Mo rich case, the chemical potential μ_{Mo} is the energy of one Mo atom in body-centered cubic structure, and the chemical potential μ_S can be calculated based on the equation (1). The neutral defect formation energies are denoted as the equation (2) [7, 8]:

$$E^f = E_{defect}^{tot} - E_0^{tot} + n_- \mu_- - n_+ \mu_+ \quad (2)$$

where E_{defect}^{tot} and E_0^{tot} are the total energy of the defective supercell and host supercell, n_- and n_+ are the number of atoms being removed and added, μ_- and μ_+ are the corresponding chemical potentials, respectively.

Under S rich conditions, one Mo vacancy defect energy in the $Mo_{15}S_{32}$ system in comparison to the ideal $Mo_{16}S_{32}$ system is obtained according to equation (1) and (2),

$$E^f = E_{Mo_{15}S_{32}} - E_{Mo_{16}S_{32}} + \mu_{Mo} \quad (3)$$

Under S rich conditions, one S intersitial defect energy in the $Mo_{16}S_{33}$ system in comparison to the ideal $Mo_{16}S_{32}$ system is obtained according to equation (1) and (2),

$$E^f = E_{Mo_{16}S_{33}} - E_{Mo_{16}S_{32}} - \mu_S \quad (4)$$

Under S rich conditions, one S_{Mo} antisite defect energy in the $Mo_{17}S_{31}$ system in comparison to the ideal $Mo_{16}S_{32}$ system is obtained according to equation (1) and (2),

$$E^f = E_{Mo_{15}S_{33}} - E_{Mo_{16}S_{32}} - \mu_S + \mu_{Mo} \quad (5)$$

Under Mo rich conditions, one S vacancy defect energy in the $Mo_{16}S_{31}$ system in comparison to the ideal $Mo_{16}S_{32}$ system is obtained according to equation (1) and (2),

$$E^f = E_{Mo_{16}S_{31}} - E_{Mo_{16}S_{32}} + \mu_S \quad (6)$$

Under Mo rich conditions, one Mo_S antisite defect energy in the $Mo_{17}S_{31}$ system in comparison to the ideal $Mo_{16}S_{32}$ system is obtained according to equation (1) and (2),

$$E^f = E_{Mo_{17}S_{31}} - E_{Mo_{16}S_{32}} + \mu_S - \mu_{Mo} \quad (7)$$

As listed in Table S5, under Mo rich condition, both formation energies of neutral S vacancy and Mo_S antisite defects are smaller than the defect energies under S rich condition, suggesting the defects are more energetically favorable under Mo condition.

In addition, the neutral S vacancy is in favor of lowest defect formation energy among the various types of defects being studied.

Table S5. The calculated defect formation energies (E^f) of intrinsic defects of monolayer MoS_2.

defect	S rich			Mo rich	
type	Mo vacancy	S_i interstitial	S_{Mo} antisite	S vacancy	Mo_S antisite
E^f(eV)	4.46	7.70	4.22	1.26	3.83

Owing to Mo_S antisite defect in favor of the highest spin polarization in contrast to the other defects, we study the effect of Y/Yb dopant on the Mo_S antisite defect formation energy. Defect formation energies of the Mo_S antisite defect for the monolayer $Mo_{17}S_{31}$ with one Mo_S antisite, $Mo_{16}YS_{31}$ with one Mo_S antisite and one Y dopant, $Mo_{16}YbS_{31}$ with one Mo_S antisite and one Yb dopant are calculated.

For monolayer $Mo_{16}YS_{31}$ system with one Mo_S antisite and one Y dopant, the Mo_S antisite formation energy is calculated according to equation (1) and (2),

$$E^f = E_{Mo_{16}YS_{31}} - E_{Mo_{15}YS_{32}} + \mu_S - \mu_{Mo} \quad (8)$$

For monolayer $Mo_{16}YbS_{31}$ system with one Mo_S antisite and one Yb dopant, the Mo_S antisite formation energy is computed according to equation (1) and (2),

$$E^f = E_{Mo_{16}YbS_{31}} - E_{Mo_{15}YbS_{32}} + \mu_S - \mu_{Mo} \quad (9)$$

The computed Mo_S antisite defect formation energies of monolayer $Mo_{16}YS_{31}$, and $Mo_{16}YbS_{31}$ systems are 2.52, and 2.51 eV lower than 3.83 eV of Mo_S antisite defect in

$Mo_{17}S_{31}$ system, separately. Therefore, dopant Yb and Y can both lower the Mo_S antisite defect formation energy to enhance the spin polarization of monolayer MoS_2.

References

1. Z. Yuan and N. Li, *RSC Adv.*, 2016, **6**, 92048-92056.
2. C. N. M. Ouma, K. O. Obodo, M. Braun and G. O. Amolo, *J. Mater. Chem. C*, 2018, **6**, 4015-4022.
3. C. N. M. Ouma, S. Singh, K. O. Obodo, G. O. Amolo and A. H. Romero, *Phys. Chem. Chem. Phys.*, 2017, **19**, 25555-25563.
4. Z. Rák and D. W. Brenner, *Philos. Mag.*, 2015, **95**, 2167-2174.
5. D. Wang, W. Ju, T. Li, Q. Zhou, Z. Gao, Y. Zhang and H. Li, *J. Phys. Chem. Solids*, 2019, **131**, 119-124.
6. J. C. Wu, J. W. Zheng, P. Wu and R. Xu, *J. Phys. Chem. C*, 2011, **115**, 5675-5682.
7. H. Cheng, J. Zhou, M. Yang, L. Shen, J. Linghu, Q. Wu, P. Qian and Y. P. Feng, *J. Mater. Chem. C*, 2018, **6**, 8435-8443.
8. K. Iordanidou, M. Houssa, J. Kioseoglou, V. V. Afanas'ev, A. Stesmans and C. Persson, *ACS Appl. Nano Mater.*, 2018, **1**, 6656-6665.